Applied Surface Science 307 (2014) 46–51

Contents lists available at ScienceDirect

Applied Surface Science

journal homepage: www.elsevier.com/locate/apsusc

Size distributions of fullerene surface clusters

N.V. Sibirev[a,b,*], V.G. Dubrovskii[a,c,d], A.V. Matetskiy[e,f], L.V. Bondarenko[e,f], D.V. Gruznev[e,f], A.V. Zotov[e,f,g], A.A. Saranin[e,f]

[a] St. Petersburg Academic University, Khlopina 8/3, 194021 St. Petersburg, Russia
[b] St. Petersburg State Polytechnical University, Politechnicheskaya 29, 195251 St. Petersburg, Russia
[c] Ioffe Physical Technical Institute of the Russian Academy of Sciences, Politekhnicheskaya 26, 194021 St. Petersburg, Russia
[d] St. Petersburg State University, Physical Faculty, Ulianovskaya Street 3, Petrodvorets, 198504 St. Petersburg, Russia
[e] Institute of Automation and Control Processes FEB RAS, Radio 5, 690041 Vladivostok, Russia
[f] Far Eastern Federal University, School of Natural Sciences, 690950 Vladivostok, Russia
[g] Vladivostok State University of Economics and Service, Department of Electronics, 690600 Vladivostok, Russia

ARTICLE INFO

Article history:
Received 10 December 2013
Received in revised form 4 March 2014
Accepted 20 March 2014
Available online 30 March 2014

Keywords:
Fullerene
Nucleation
Surface islands

ABSTRACT

We present an exactly solvable generalization of the rate equation model for irreversible growth with size-independent capture numbers which includes desorption of monomers. It is shown that the universal size distribution shapes depend on the sole parameter, the ratio between the characteristic diffusion and adsorption areas. We perform a statistical analysis of the scanning tunneling microscopy images of C_{60} clusters deposited onto In-modified Si(1 1 1)$\sqrt{3} \times \sqrt{3}$-Au surfaces at different temperatures and deduce the experimental size distributions. These distributions have an essentially asymmetric shape with a much faster decay toward larger sizes. Fitting the data with theoretical distribution shapes yield the estimates for some important kinetic parameters, in particular, the temperature-dependent diffusion lengths and effective lifetimes of C_{60} monomers.

1. Introduction

Studies of size distributions of different "clusters" such as three-dimensional droplets [1], two-dimensional (2D) or three-dimensional surface islands [2–16] and one-dimensional nanowires [17] or linear peptide chains [18] is paramount for understanding their growth behavior as well as the resulting physical properties of the cluster ensembles. Theoretical approaches based on classical nucleation theory [1,4,5,19] apply whenever the clusters of interest consist of at least several tens of monomers and are terminated by distinct boundaries with a metastable phase. Such systems can be well described within the frame of classical approach involving macroscopic approximations for the formation energy and a continuum kinetic equation for time-dependent distribution of nuclei over sizes, coupled with the material balance.

In many cases, however, we deal with particles consisting of only a few monomers, while the decay of clusters can be neglected on a time scale of interest. In this case, the cluster formation is described within the mean field approach with discrete rate equations for irreversible growth [2,3,6–16,20,21], accounting for the influx and sink of monomers as well as for their consumption by growing clusters. For surface islands, the material influx is due to vapor deposition, while the sink originates from desorption from a substrate surface [15]. Irreversible growth models are much simpler for the analysis and may be even solved exactly for some particular forms of the capture numbers. On the other hand, continuum approximation is irrelevant for small clusters. Also, the mean treatment fails when subtle correlations between island size and separation affect the effective capture numbers and thus control the size distribution shapes. Comprehensive reviews of the advances in the theory of submonolayer surface growth, covering the mean field rate equations as well as a more complex approaches for the island size distribution can be found, e.g., in Refs. [9,21].

Here, we present an exactly solvable generalization of the discrete irreversible growth model for 2D islands with size-independent capture numbers (such a model was considered earlier, e.g., by Bartelt and Evans [7]), with desorption included. We show that the distribution shapes are determined by the sole dimensionless parameter, a combination of the deposition rate, the lifetime before desorption and the effective diffusion length of monomers. A more general theoretical analysis in the case of scaling size dependences of the capture numbers in systems with desorption, along with a discussion of the asymptotic scaling properties [7,9,21] is given in Ref. [20].

* Corresponding author at: St. Petersburg Academic University, Khlopina 8/3, 194021 St. Petersburg, Russia. Tel.: +7 9112827886.
E-mail addresses: NickSibirev@yandex.ru, NickSibirev@list.ru (N.V. Sibirev).

http://dx.doi.org/10.1016/j.apsusc.2014.03.132
0169-4332/

Experimental part of the work deals with C_{60} fullerene clusters deposited onto In-modified Si(1 1 1)$\sqrt{3}\times\sqrt{3}$-Au surfaces at different temperatures and then characterized by scanning tunneling microscopy (STM) [22–25]. Statistical analysis of STM images enables a precise determination of not only the temperature-dependent average size and density of clusters, but also of the size distributions. We find that the density of C_{60} clusters decreases and their average size increases as the surface temperature increases, while the size distributions have an essentially asymmetric shape. We then fit the experimental size spectra with our model solutions and show a reasonable correlation of the results in all the cases considered. These fits allow us to estimate some important kinetic parameters of C_{60} monomers such as diffusion lengths, effective lifetimes and activation energies.

2. Theoretical model of irreversible growth

In modeling of time-dependent concentrations $n_s(t)$ of the immobile surface clusters A_s consisting of s monomers (size s for brevity), we assume that the clusters are fed by surface diffusion of the mobile monomers A_1 that have the diffusion coefficient D, arrive onto the surface at the time-independent rate F and desorb from the surface with the characteristic time t_{des}. We neglect the decay of clusters on the time scale of interest, in which case the number of monomers in the critical cluster equals one and the cluster growth proceeds irreversibly: $A_s + A_1 \rightarrow A_{s+1}$, with $i = 1, 2, 3\ldots$. The rate equations describing such an irreversible growth write down as [2,3,6–16,18,20,21]

$$\frac{dn_1}{dt} = F - \frac{n_1}{t_{des}} - 2D\sigma_1 n_1^2 - Dn_1\sum_{s=2}^{\infty}\sigma_s n_s; \tag{1}$$

$$\frac{dn_s}{dt} = Dn_1(\sigma_{s-1}n_{s-1} - \sigma_s n_s) \qquad s\geq 2, \tag{2}$$

with σ_s as the corresponding capture numbers. Eq. (1) shows that the concentration of free monomers on the substrate surface changes due to their adsorption, desorption and consumption by the growing clusters, where the dimer formation requires two monomers. The chain of Eq. (2) shows that the concentration n_s for each $s \geq 2$ increases when monomers attach to $s-1$-mers and decreases when monomers attach to s-mers. Summing up Eq. (2) for all $s \geq 2$, the surface density of clusters, $N = \sum_{s=2}^{\infty} n_s$, obeys the equation

$$\frac{dN}{dt} = D\sigma_1 n_1^2, \tag{3}$$

which gives the nucleation rate in irreversible growth. These rate equations should be solved with boundary conditions $n_s(t=0) = 0$ for all $s \geq 1$, i.e., neither monomers nor clusters are present at the beginning of deposition.

In our further analysis, we assume that $\sigma_s = \sigma_* = const$ for all $s \geq 2$ in the first approximation, so that each monomer is attached to a cluster with the size-independent sticking probability σ_* when they meet. However, the capture number for adatoms σ_1 can be different from σ_*. In this case, Eqs. (1)–(3) are considerably simplified and can be put in the dimensionless form by introducing the dimensionless time $\tau = t/t_{des}$, the effective monomer diffusion length $\lambda = \sqrt{\sigma_* D t_{des}}$ (accounting for the capture number σ_*), the normalized cluster concentrations $f_s = \lambda^2 n_s$, the surface density $G = \lambda^2 N$, and the new time-dependent variable z by definition

$$\frac{dz}{d\tau} = f_1, \quad z(\tau = 0) = 0. \tag{4}$$

Since all the growth rates now equal f_1 and are s-independent, the physical meaning of the z variable is very simple [20]: it corresponds to the right boundary of the size distribution (i.e., to the maximum possible size of clusters having emerged at $\tau = 0$) in the deterministic limit, where the SD shape is not affected by kinetic fluctuations [19].

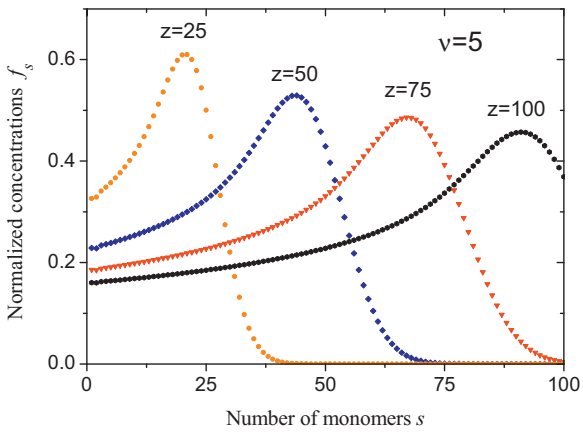

Fig. 1. Normalized concentrations f_s at the fixed growth conditions ($\nu = 1$) and different z relating to different growth times.

In these variables, Eq. (1) for the monomer concentration and Eq. (3) for the island density become

$$\frac{df_1}{d\tau} = \nu - f_1 - 2bf_1^2 - f_1 G; \tag{5}$$

$$\frac{dG}{d\tau} = bf_1^2, \tag{6}$$

with $f_1(\tau = 0) = G(\tau = 0) = 0$. Here, the coefficient $b = \sigma_1/\sigma_*$ accounts for different capture number for adatoms and clusters. The control parameter ν is defined as follows:

$$\nu = \lambda^2 F t_{des} = \sigma_* D F t_{des}^2, \tag{7}$$

and has clear meaning of the number of monomers arriving from the vapor flux F onto the surface area $\lambda^2 = \sigma_* D t_{des}$ during the time interval t_{des}.

Eq. (2) for the cluster concentrations become linear in terms of the z variable:

$$\begin{aligned} \frac{df_2}{dz} &= bf_1 - f_2 \\ \frac{df_s}{dz} &= f_{s-1} - f_s, \quad s\geq 3. \end{aligned} \tag{8}$$

The exact solutions to this system are easily obtained by introducing the generating function for concentrations, as in Ref. [7]:

$$f_{s+2}(z) = \frac{b}{s!}\int_0^z dx f_1(z-x)x^s e^{-x}, \quad s\geq 0. \tag{9}$$

Here, the normalized concentration of free monomers f_1 is obtained as a function of τ from Eqs. (5) and (6) and then inverted as a function of z by means of Eq. (4). This solution generalizes the earlier result of Bartelt and Evans [7] to systems with desorption, and is presented in terms of the z variable which is more convenient for further analysis.

The discrete size distributions of differently sized clusters, computed from Eqs. (4) and (9), are shown in Figs. 1 and 2, for different deposition times (z) and deposition conditions (ν), respectively. Here and below, we put $b = 1$ in calculations, however, reasonable variation of b does not strongly affect the spectrum shapes. It is seen that the size distributions always have essentially asymmetric shapes, with an abrupt right tail and a much slower regression toward smaller i. It is noteworthy that these distributions are universal and depend on the sole parameter ν, while fitting a particular

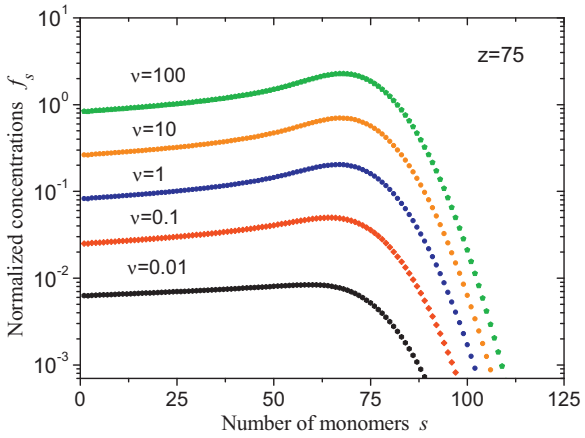

Fig. 2. Normalized concentrations f_s at a given growth time relating to $z = 80$ for different growth conditions (ν).

growth experiment just needs re-scaling of the results with the adjustable values of λ and z.

3. Experiments on C_{60} cluster growth on (Au, In)/Si(1 1 1) surface

We now consider the ensembles of C_{60} surface clusters formed upon deposition of C_{60} molecules onto the In-modified Si(1 1 1)$\sqrt{3} \times \sqrt{3}$-Au surface. This interesting system has recently been characterized in a number of works by using STM technique [22–25]. Concerning the substrate surface itself, it has been shown that while the Si(1 1 1)$\sqrt{3} \times \sqrt{3}$-Au surface is structurally poor due to the presence of random domain wall networks [26], it can be drastically improved by adsorbing small amounts of In [22]. The resultant surface appears to be highly ordered homogeneous and almost defect-free [22], which makes it a good prototype substrate for studying the island growth processes. When C_{60} molecules are deposited onto this surface, they self-assemble into 2D clusters due to the thermally activated surface diffusion of fullerene monomers. Within the clusters, the fullerenes are arranged into the close-packed hexagonal arrays.

The growth behavior and morphology of C_{60} clusters on the (Au, In)/Si(1 1 1) surfaces have been studied in our recent paper [25], where the dependencies of the cluster density on the growth temperature and the deposition rate have been analyzed and the C_{60} surface migration has been simulated using density functional theory calculations. The critical island size $i_c = 1$ (the case corresponding to irreversible island growth) was found in the entire temperature range from 109 to 240 K. However, two temperature intervals, from 109 to 140 K and from 160 to 240 K, were distinguished as governed by different diffusion mechanisms. In the present study, we restrict our analysis to only the low-temperature interval (109–140 K). The actual behavior of the C60/Si(1 1 1))$\sqrt{3} \times \sqrt{3}$-(Au, In) system at low temperatures is believed to meet the core assumptions of the above model: (i) irreversible growth; (ii) size-independent capture numbers (due to a rather small number of monomers in the clusters studied) and (iii) no transformation of size distribution shapes after growth. This is apparently not the case for the high-temperature interval, where such effects as the post-growth ripening and the formation of magic clusters become substantial [25].

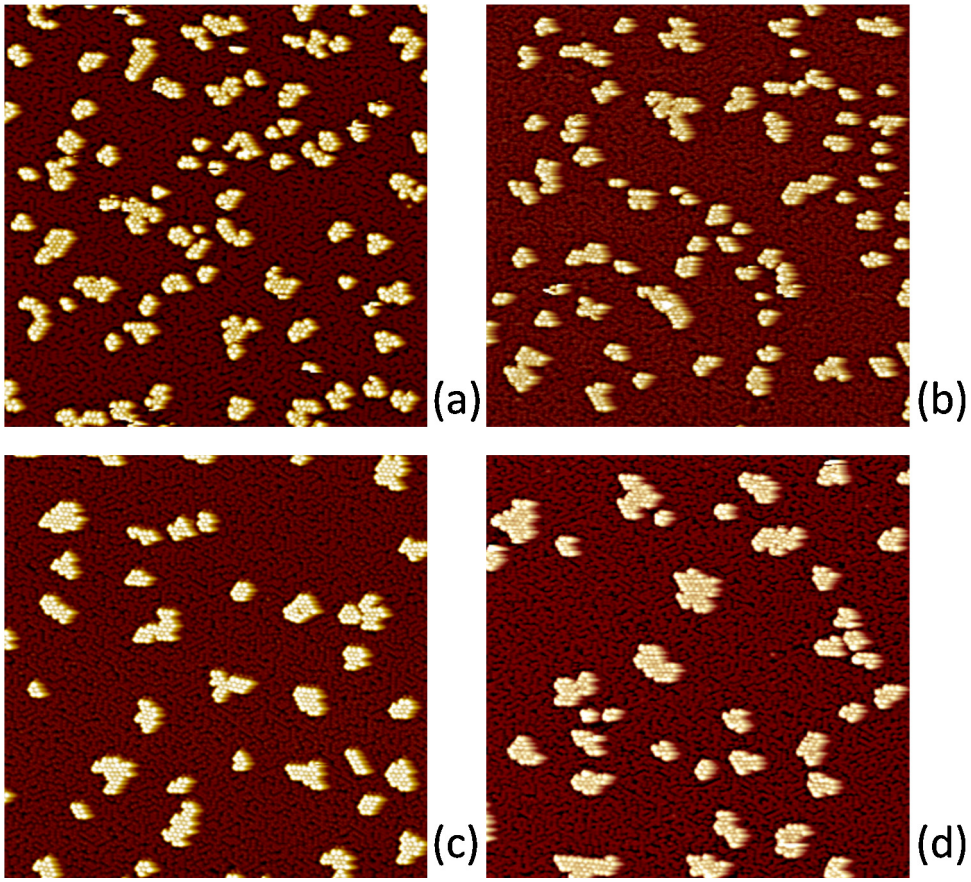

Fig. 3. 88 nm × 88 nm STM images ($Vs = -2$ V, $I = 0.8$ nA) of C_{60} clusters formed upon C_{60} deposited onto In-modified Si(1 1 1)$\sqrt{3} \times \sqrt{3}$-Au surface held at different temperatures, (a) 109 K, (b) 118 K, (c) 130 K, and (d) 139 K.

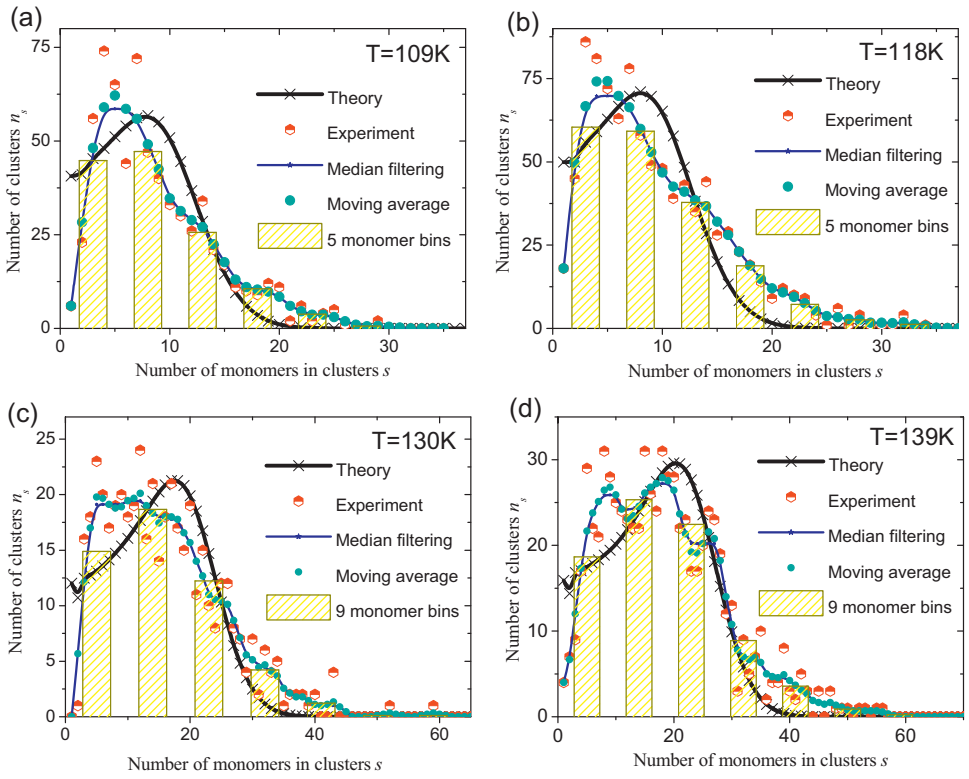

Fig. 4. Size histograms of fullerene clusters in samples (a) to (d) deposited at different surface temperatures, fitted by the theoretical size distributions (black curves) with the fitting parameters listed in Table 1.

Fig. 3 shows typical STM images of the C60 clusters obtained at four different temperatures: 109, 118, 130, and 139 K. Similar images, usually acquired from a larger surface area, were used for statistical analysis to deduce the experimental cluster size distributions over i. Since each fullerene within any cluster is well-resolved by our STM, the number of C_{60} monomers in a given cluster was determined with a single-fullerene accuracy.

4. Results and discussion

Experimental distributions of the number n_s of differently sized fullerene clusters over s (per the scan area of 106,000 nm^2), obtained at the different surface temperatures from 109 to 139 K after 480 s of deposition, are shown by red symbols in Fig. 4. We also present different smoothed distributions: the moving average $[\tilde{n}_s = (n_{s-2} + 2n_{s-1} + 3n_s + 2n_{s+1} + n_{s+2})/9)]$, the moving average with the median filtering, and the histogram showing the average number of clusters within 5 monomer bins. These data are also shown in Fig. 4, with the experimental deposition conditions (surface temperature T, deposition rate F and deposition time t) and the corresponding scan areas S summarized in Table 1.

Theoretical fits shown in Fig. 4 were obtained from Eqs. (4), (5), (6) and (9) as follows. The z and ν values were varied and the dimensionless concentrations f_s were calculated numerically related to the growth time $t = 480$ s and the experimental deposition rates F. After that, the normalization factor S/λ^2 was obtained by the least square method to ensure the best fits to the experimental size spectra n_s. This procedure allowed us to find not only the effective diffusion length λ, but also the "effective" diffusion coefficient $\sigma_* D$ and the lifetime of the fullerene monomers before desorption t_{des} at different temperatures. Unfortunately, it was impossible to decouple the sticking coefficient σ_* and the surface diffusivity D, since they enter all the growth equations only in composition. The best fitting values of ν and z, along with the values of $\sigma_* D$, t_{des} and λ deduced from the fits, are given in Table 1 for each temperature. The fits yield reasonable estimates for the effective diffusion coefficient of the order of 10^{-13} to 10^{-11} cm^2/s, the effective diffusion length of the order of several tens of nanometers and the monomer lifetime of the order of several tens of seconds, depending on the surface temperature. As expected, the $\sigma_* D$ increases and t_{des} decreases toward higher temperatures.

From Fig. 5, the fullerene clusters grow much larger at higher temperatures, with the most representative number of monomers in clusters increasing from ~10 at 109 K ~25 at 139 K. This process is associated with the corresponding decrease of the cluster density, because the total amount of deposited fullerenes is almost the same for all the samples and the fraction of desorbed monomers is not dominant (the estimated values of ν range from 2 to 6 in all cases). Theoretical fits represent quite well these tendencies. It is also seen that the experimental size distributions generally follow the theoretical asymmetric shapes with a faster decay toward larger s. However, the theoretical asymmetry is usually more

Table 1
Experimental conditions and fitting parameters of the size distributions of fullerene clusters at different temperatures.

No.	T (K)	F (nm^{-2} s^{-1})	t (s)	S (nm^2)	ν	z	$\sigma_* D$ (nm^2 s^{-1})	t_{des} (s)	λ (nm)
(a)	109	0.000172	480	70,300	2.17	10.6	6.2	45.0	16.7
(b)	118	0.000173	480	105,900	3.2	10.8	9.5	44.3	20.5
(c)	130	0.000132	480	116,500	5	21.6	76.9	22.2	41.3
(d)	139	0.000152	480	180,600	6	24.7	106	19.4	45.3

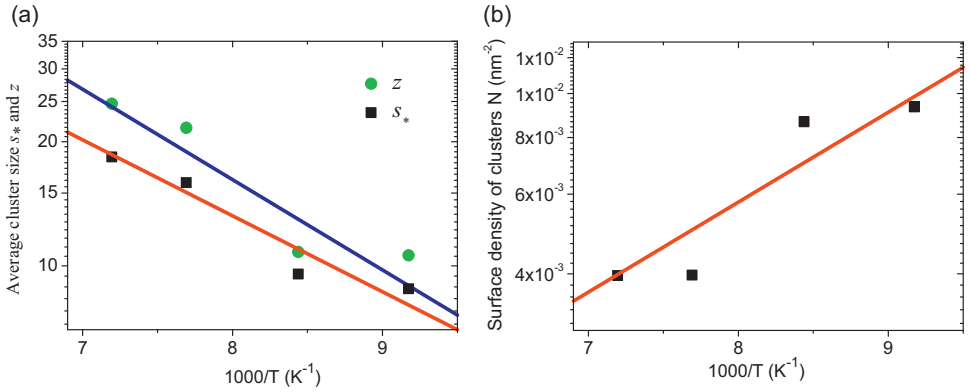

Fig. 5. Arrhenius fits (lines) of the fitting parameter z and the experimental average size s_* (a), and surface density (b) of fullerene clusters (squares) versus inverse temperature.

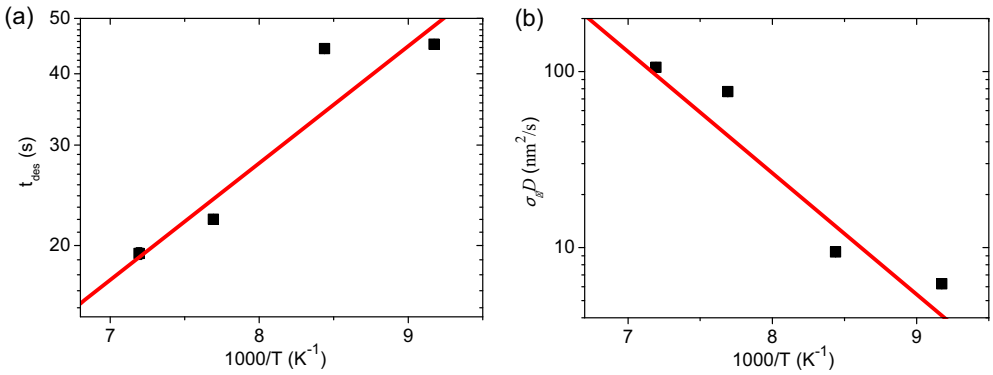

Fig. 6. Arrhenius plots (lines) for the fitting values of t_{des} (a) and $\sigma_* D$ (b) (symbols).

pronounced that the experimental one. The discrepancies should be due to a simplified theoretical model which does not account for the dependencies of the capture numbers on the cluster size and coverage. This remains to be studied.

Fig. 6 shows that the temperature dependences of the fitting parameter z, the average size $s_* = \sum_{i=2}^{\infty} s n_s / N$ and the surface density N of fullerene clusters generally follow the Arrhenius-like behavior, which is of course not surprising. Fig. 6 shows the similar Arrhenius-like temperature dependences of the fitting values t_{des} and $\sigma_* D$ from Table 1. The parameters of the Arrhenius fits $p = A_p \exp(\pm E_p / k_B T)$ (with E_p as the activation energy, k_B as the Boltzmann constant and A_p as the corresponding pre-exponential factor) for different parameters given in Table 1 ($p = s_*, z, N, t_{des}, \sigma_* D, \lambda$) are summarized in Table 2.

In Ref. [27], the diffusion of C_{60} molecules on large, atomically flat terraces of the insulating $CaF_2(1\,1\,1)$ surface was studied at different substrate temperatures below room temperature. Based on the analysis of spatial properties of clusters created by nucleation of diffusing C_{60} molecules, the critical size i_c was determined to equal one, as in our study. Further, the diffusion barrier of $E_D = (214 \pm 16)$ meV was obtained by analyzing the island densities at different substrate temperatures. Our E_D is noticeably smaller, only 137 meV, meaning that the diffusion of C60 molecules on the In-modified Si(1 1 1)$\sqrt{3} \times \sqrt{3}$-Au surfaces is faster in these conditions (with the same order of the attempt frequencies).

To conclude, we have presented the experimental data on the STM imaging of C_{60} fullerene clusters deposited onto In-modified Si(1 1 1)$\sqrt{3} \times \sqrt{3}$-Au surface, which allows a precise determination of the cluster size spectra at different surface temperatures between 109 and 139 K. Our irreversible growth model has an interesting semi-analytical solution and fits fairly well the experimental distribution shapes. Theoretical fits enables us to deduce some important kinetic parameters such as the effective diffusion coefficients, diffusion lengths and adatom lifetimes. It has been shown that the cluster size increases and their surface density decreases with temperature, both following the Arrhenius behavior. We now plan to perform more growth experiments, characterization and a more advanced modeling (including studies of peculiar island morphologies [28], "magic clusters" [25] and fluctuation-induced effects [29]) for this important system to identify more control tools for tuning the size distribution of fullerene clusters.

Table 2
Parameters of the Arrhenius fits for different temperature-dependent values.

Value	Activation energy E_p (meV)	Pre-exponent A_p
Average size s_*	37	393
z	43	912
Surface density N (nm^{-2})	39	1.5×10^{-4}
Characteristic lifetime t_{des} (s)	41	0.64
Effective diffusion coefficient $\sigma_* D$ (nm^2 s^{-1})	137	8.7×10^6
Effective diffusion length λ (nm)	48	2429

Acknowledgements

This work was partially supported by grants of the Russian Foundation for Basic Research and the FP7 project NANOEMBRACE. NVS gratefully acknowledges support from the grant council of President of the Russian Federation SP-386.2012.1 for young scientists.

References

[1] F.M. Kuni, A.K. Shchekin, A.P. Grinin, Phys. Usp. 171 (2001) 345.
[2] J.A. Venables, Philos. Mag. 27 (1973) 697.

[3] S. Stoyanov, D. Kashchiev, Curr. Top. Mater. Sci. 7 (1981) 69.
[4] D. Kashchiev, Nucleation: Basic Theory with Applications, Butterworth-Heinemann, Oxford, 2000.
[5] A.V. Osipov, F. Schmitt, S.A. Kukushkin, P. Hess, Appl. Surf. Sci. 188 (2002) 156.
[6] J.A. Venables, G.D.T. Spiller, M. Hanbucken, Rep. Prog. Phys. 47 (1984) 399.
[7] M.C. Bartelt, J.W. Evans, Phys. Rev. B 46 (1992) 12675.
[8] M.C. Bartelt, M.C. Tringides, J.W. Evans, Phys. Rev. B 47 (13) (1993) 891.
[9] J.W. Evans, P.A. Thiel, M.C. Bartelt, Surf. Sci. Rep. 61 (2006) 1.
[10] G.S. Bales, A. Zangwill, Phys. Rev. B 55 (1997) R1973.
[11] G.S. Bales, D.C. Chrzan, Phys. Rev. B 50 (1994) 6057.
[12] F.G. Gibou, C. Ratsch, M.F. Gyure, S. Chen, R.E. Caflisch, Phys. Rev. B 63 (2001) 115401.
[13] M. Korner, M. Einax, P. Maass, Phys. Rev. B 86 (2012) 085403.
[14] D.D. Vvedensky, Phys. Rev. B 62 (2000) 15435.
[15] P. Jensen, H. Larralde, A. Pimpinelli, Phys. Rev. B 55 (1997) 2556.
[16] W. Dieterich, M. Einax, P. Maass, Eur. Phys. J. Spec. Top. 161 (2008) 151.
[17] V.G. Dubrovskii, Phys. Rev. B 87 (2013) 195426.
[18] V.G. Dubrovskii, N.V. Sibirev, I.E. Eliseev, S.Yu. Vyazmin, V.M. Boitsov, Yu.V. Natochin, M.V. Dubina, J. Chem. Phys. 138 (2013) 244906.
[19] V.G. Dubrovskii, J. Chem. Phys. 131 (2009) 164514.
[20] V.G. Dubrovskii, N.V. Sibirev, Phys. Rev. B 89 (2014) 054305.
[21] M. Einax, W. Dieterich, P. Maass, Rev. Mod. Phys. 85 (2013) 921.
[22] D.V. Gruznev, I.N. Filippov, D.A. Olyanich, D.N. Chubenko, I.A. Kuyanov, A.A. Saranin, A.V. Zotov, V.G. Lifshits, Phys. Rev. B 73 (2006) 115335.
[23] A.V. Matetskiy, D.V. Gruznev, A.V. Zotov, A.A. Saranin, Phys. Rev. B 63 (2011) 105421.
[24] D.V. Gruznev, A.V. Matetskiy, L.V. Bondarenko, O.A. Utas, A.V. Zotov, A.A. Saranin, J.P. Chou, C.M. Wei, M.Y. Lai, Y.L. Wang, Nat. Commun. 4 (2013) 1679.
[25] A.V. Matetskiy, L.V. Bondarenko, D.V. Gruznev, A.V. Zotov, A.A. Saranin, J.P. Chou, C.R. Hsing, C.M. Wei, Y.L. Wang, Surf. Sci. 616 (2013) 44.
[26] T. Nagao, S. Hasegawa, K. Tsuchie, S. Ino, C. Voges, G. Klos, H. Pfnur, M. Henzler, Phys. Rev. B 57 (1998) 10100.
[27] F. Loske, J. Lübbe, J. Schütte, M. Reichling, A. Kühnle, Phys. Rev. B 82 (2010) 155428.
[28] M. Körner, F. Loske, M. Einax, A. Kühnle, M. Reichling, P. Maass, Phys. Rev. Lett. 107 (2011) 016101.
[29] V.G. Dubrovskii, M.V. Nazarenko, J. Chem. Phys. 132 (2010) 114507.